Data-based autonomously discovering method for nonlinear aerodynamic force of quasi-flat plate

ⓘ Teng Ma (马腾), ⓘ Wei Cui (崔巍), ⓘ Tingting Gao (高婷婷), et al.

View Online   Export Citation   CrossMark

ARTICLES YOU MAY BE INTERESTED IN

A POD-DMD augmented analysis procedure to isolating dominant flow field structures in a street canyon
Physics of Fluids (2023); https://doi.org/10.1063/5.0133375

Investigation of winglets for better control over drag and lift coefficients for commercial aircrafts
AIP Conference Proceedings **2643**, 050063 (2023); https://doi.org/10.1063/5.0112377

Numerical investigations of vortex dynamics and loss generation in the corner separation region of a high subsonic compressor blade
Physics of Fluids **35**, 025104 (2023); https://doi.org/10.1063/5.0134670

Physics of Fluids

Special Topic: Paint and Coating Physics

Submit Today!

Data-based autonomously discovering method for nonlinear aerodynamic force of quasi-flat plate

Teng Ma (马腾),[1] Wei Cui (崔巍),[1,2,a] Tingting Gao (高婷婷),[3,4] Shengyuan Liu (刘圣源),[5] Lin Zhao (赵林),[1,2] and Yaojun Ge (葛耀君)[1,2]

AFFILIATIONS

[1]State Key Lab of Disaster Reduction in Civil Engineering, Tongji University, Shanghai 200092, People's Republic of China
[2]Key Laboratory of Transport Industry of Wind Resistant Technology for Bridge Structures, Tongji University, Shanghai 200092, People's Republic of China
[3]School of Physical Science and Engineering, Tongji University, Shanghai 200092, People's Republic of China
[4]State Key Laboratory of Intelligent Autonomous Systems, Frontiers Science Center for Intelligent Autonomous Systems, and Shanghai Research Institute for Intelligent Autonomous Systems, Tongji University, Shanghai 200092, People's Republic of China
[5]Huaneng Clean Energy Research Institute, Beijing 102209, People's Republic of China

[a]Author to whom correspondence should be addressed: cuiwei@tongji.edu.cn

ABSTRACT

Expression of nonlinear aerodynamic phenomena and calculation of nonlinear aeroelastic response require accurate and concise aeroelastic force function. In this paper, a group sparse regression method is used to reveal the nonlinear mapping aerodynamics relationship between motion and force from data. The aeroelastic force function discovered by this method balances modeling accuracy and simplicity. A quasi-flat plate in coupled vertical–torsional harmonic motion is employed as an experimental object in this work. Aerodynamic motion-force dataset is collected by forced motion test in wind tunnel, including 484 cases. The sparse regression analytic result shows that $\alpha\dot{\alpha}, \alpha^3, \dot{\alpha}^3$ (α is torsional displacement) can represent the nonlinearity in aerodynamic for all cases, even wind speed, amplitude, amplitude ratio, frequency ratio, and angle of attack are in different combinations.

Published under an exclusive license by AIP Publishing. https://doi.org/10.1063/5.0133526

I. INTRODUCTION

The unsteady aerodynamic model is a core equation for wind-induced vibration analysis (Gülçat, 2010; Curtiss, Jr. *et al.*, 2013). For engineering practice, accurate and concise aerodynamic model is important for aeroelastic stability analysis and structural shape optimization (Yang and Zhao, 1988; Dinyavari and Friedmann, 1986; and Chen *et al.*, 2000). Mechanistically, it also illustrates how the wind-induced instability occurs (like flutter) (Theodorsen and Mutchler, 1935; Thomas *et al.*, 2002). Interests in unsteady aerodynamics have been continuously increasing over the last several decades. There are currently two main approaches in unsteady aerodynamic modeling: (1) deriving equations from basic fluid principles and a series of assumptions, and (2) semi-empirical data-driven model. These two approaches are generally used to develop a motion-to-force model.

Since 1920s, classical unsteady aerodynamic theories are based on a series of assumptions (Birnbaum, 1924; Prandtl, 1924): for a high-Reynolds-number, small-angle-of-attack (AoA) incompressible flow around an infinitely thin airfoil, sheets of vorticity are shed from

sharp edges only, and the flow outside of these sheets can be considered irrotational. Under these assumptions, unsteady aerodynamic force is calculated by simultaneously solving the linear Laplace equation and Kutta condition, such as simple harmonic oscillation lift frequency response (Theodorsen and Mutchler, 1935), impulsively started lift step response (Wagner, 1925), and gust problem (von Karman and Sears, 1938). Facing specific physical problems, Theodorson *et al.* first presented the expressions of aerodynamic lift and moment. Although it cannot keep accuracy under all conditions, it still acts as the pillars in many engineering analyses. After that, there are also lots of aerodynamic modeling research considering leading-vortex (Ellington, 1984; Wang and Eldredge, 2013; and Xia and Mohseni, 2017) and viscous (Brown and Daniels, 1975; Taha and Rezaei, 2019). These novel models can give results, which are more close to the reality, but they are not widely used in engineering calculation, because the theory becomes difficult to derive after relaxing the assumptions and too complex to solve aeroelastic problem. Those methods try to propose a numerical simulation governing equation

not an explicit formula. Obviously, the later one is needed in solving dynamic problem.

Theoretical methods always take the flat plate with unsteady motion as basic research object and relax the above assumptions step by step. However, there are lots of complex geometries, which are required to consider aerodynamic and aeroelastic problems in real world, not only flat plate. The semi-empirical modeling method has been becoming popular to solve engineering problems. A classic example is flutter derivatives (Scanlan and Tomko, 1971), which is the most widely used theory in bridge wind-resistant design, since the failure of Old Narrow Tacoma Bridge (Amman et al., 1941). Scanlan (2002) built unsteady aerodynamic force expression for any geometrical shape inspired by the style of Theodorson's model. It is assumed that the aerodynamic force is the linear function of motion for flat plate and other geometries. The parameters of the flat plate are known from Theodorson's model, while parameters are unknown for other shapes. The flutter derivatives are identified from wind tunnel test data or computational fluid dynamics (CFD) simulation (Gu et al., 2000; Sarkar et al., 1992; Chen et al., 2002; Fang et al., 2020; and Chu et al., 2022). The aerodynamic force expression format with undetermined parameters is sufficient and more effective for engineering practice.

The development progress of semi-empirical method is totally different from the theoretical method. Semi-empirical expression format is from the understanding of aerodynamic force, like linear relation between aerodynamic force and motion from Theodorson's research. During several decades of research, more and more nonlinear aeroelastic phenomena have been found, like limit-cycle oscillation (Li, 1988; Denegri, Jr., 2000), multi-frequency effect (Liu et al., 2021), hysteretic phenomenon (Diana et al., 2005), and motion dependence features (Noda et al., 2003; Zhang et al., 2020). The basic awareness of aerodynamic has been transformed from linear to nonlinear. The semi-empirical data-driven model does not focus on what causes aerodynamic nonlinearity, and only trying to find out which model can fit nonlinearity well. Polynomial function (Diana et al., 2010; de Visser et al., 2009), Volterra series (Marzocca et al., 2004; Balajewicz and Dowell, 2012; and Wu and Kareem, 2013), multilayer perception (Yao and Marques, 2017; Wu and Kareem, 2013), and recurrent neural network (Li et al., 2019; Li et al., 2020; and Li et al., 2020) have been tried to fit nonlinear aerodynamic force by taking motion as input. These models show a better accuracy performance than linear model just by enlarging the size of model. The existing semi-empirical methods all give too many parameters, which use polynomials to fit the nonlinearity, because the number of terms increases exponentially with the degree of polynomials.

In order to find out the expression form of a physical phenomenon, lots of methods are proposed and need to be reviewed. Machine learning is a significant solution to fluid and dynamic system (Muravleva et al., 2018; Pawar et al., 2021; and Chen et al., 2021). Brunton et al. (2016) proposed the sparse identification of nonlinear dynamic method (SINDy). The core idea of the SINDy algorithm is that if one supplies a sufficient set of candidate functions for representing nonlinear function, then the correct terms can be identified using sparse regression. The method has been verified by classical nonlinear dynamical systems such as the Lorenz system. Klus et al. (2018) proposed an implicit identification method of the state space equation of the dynamical system and used the sequence threshold least squares method instead of Lasso regression to complete the identification,

which improved the computational efficiency and the identification accuracy of the model. Klus et al. (2018) integrated the idea of sparsity with the Koopman operator, which further improved the integrity of the linearized sparse identification of nonlinear systems from a theoretical approach. In recent years, sparsity identification methods have been widely used in various dynamic fields (Klus et al., 2020). Qiao et al. (2016) proposed a sparse identification method with enhanced regularization and a group regularization method for identifying shock loads. Chen et al. (2019) used a sparse regularization method to identify bridge influence lines, which improved the robustness to noise disturbances. In the field of bridge wind engineering, Li et al. (2019) employed the SINDy algorithm to analyze the bridge health monitoring data and identified the time-varying bridge wind vibration force system at the bridge site. The sparse regression method has great potential to find the core function of engineering from data.

In this paper, an intelligent form-finding algorithm for nonlinear aerodynamic formulas based on group sparsity regression is proposed, which can find out the most important nonlinear terms in the aerodynamic formulas from the aerodynamic motion-force dataset. The optimization algorithm for hyper-parameters and the performance metric are updated for aerodynamic modeling accuracy. Taking the quasi-flat plate in vertical and torsional coupled motion as the experimental object, the motion-aerodynamic dataset in different motion is established through forced vibration wind tunnel test. A group sparse identification algorithm is established to extract the effective terms in the nonlinear aerodynamic formula. According to the identified results, the variation law of nonlinear aerodynamic parameters with the wind speed and motion amplitude of the incoming flow is summarized. It should be noted that the purpose of this study is not discovering the "true physics" of structure–fluid interaction. The aim of this paper is to find a concise and precise mathematical expression of nonlinear aerodynamic force.

II. AERODYNAMIC MOTION-FORCE DATASET

The data considered in this work are the force and motion measurement of quasi-flat plate in coupled vertical–torsional harmonic motion. These measurements originate from physical experiments.

A. Forced motion wind tunnel setup

An aerodynamic force-motion dataset is a group of time series data, which records aerodynamic forces (lift and moment) and displacements (vertical and torsional) of a motioned object in each time step. CFD is widely used to build such a dataset in data-driven unsteady aerodynamic model research (Kou and Zhang, 2021; Li et al., 2021; Wu et al., 2020; Pawar et al., 2020; and Li et al., 2019). Wind tunnel test is the real-world aerodynamic physical process. Yet limit to the measurement, flow field information could not be recorded. In this work, only the explicit nonlinear expression of aerodynamic force and motion is the research object. The aerodynamic physical law is tried to find from the forced motion wind tunnel experiments, not the numerical simulation.

Forced vibration wind tunnel test is used to create the dataset, which can make the model move as pre-defined motion in the time domain (Fig. 1). Zhao et al. (2020) invented a novel forced motion device (Fig. 2), which was also employed in this work. The maximum vertical, lateral, and torsional displacements of device are ± 50 mm, ± 50 mm, and $360°$. The dynamic forces were measured by two

FIG. 1. TJ-7 boundary layer wind tunnel.

FIG. 3. Geometrical configuration of the quasi-flat plate (unit: mm).

six-component high-frequency force balances produced by ATI company. The vertical and torsional limits of the balance are ± 65 N and ± 5 N m, respectively, and the maximum error is 0.1%. The displacement measurement was carried out by using two laser displacement sensors (Japan Panasonic HL-C235CE-W), with 8-μm resolution and $\pm 0.08\%$ linearity error. The sampling frequency of force and displacement signals during tests was 512 Hz. All forced motion tests were implemented in TJ-7 boundary layer wind tunnel, a simple straight-flow wind tunnel with a test section of 0.65 m wide, 3.2 m long, and 1.2 m high. TJ-7 boundary layer wind tunnel is shown in Fig. 1. The wind speed ranges from 1.0 m/s to 15.0 m/s and can be continuously adjusted. Uniform flow quality in this study is under control, the turbulence $I_u < 1\%$.

The quasi-flat plate sectional model is fabricated by carbon fiber with a total weight of 0.82 kg. The model is 0.25 m wide, 0.004 m high,
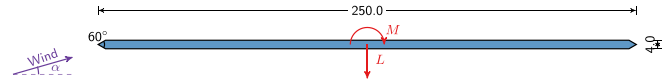
and 0.75 m long with an aspect ratio of 62.5:1, and 60° chamfer is installed on both sides of the model. Geometry and force axis are shown in Fig. 3. Two end plates parallel to the inflow direction are attached at the end of the model to ensure two-dimensional assumption. The model and forced motion device were connected by two balances and a group of connectors.

During wind tunnel test, balances measure the lift and torque force during the motion of the quasi-flat plate, including inertial and aerodynamic force. The same motion processes are run twice by the device under a certain wind speed and still air condition. The "wind–nowind" method is adopted to exclude other effect and extract aerodynamic (Diana *et al.*, 2004). Generally, the forces can be dimensionless as follows:

$$C_M = \frac{M}{\frac{1}{2}\rho U^2 B^2}, \quad C_L = \frac{L}{\frac{1}{2}\rho U^2 B}, \tag{1}$$

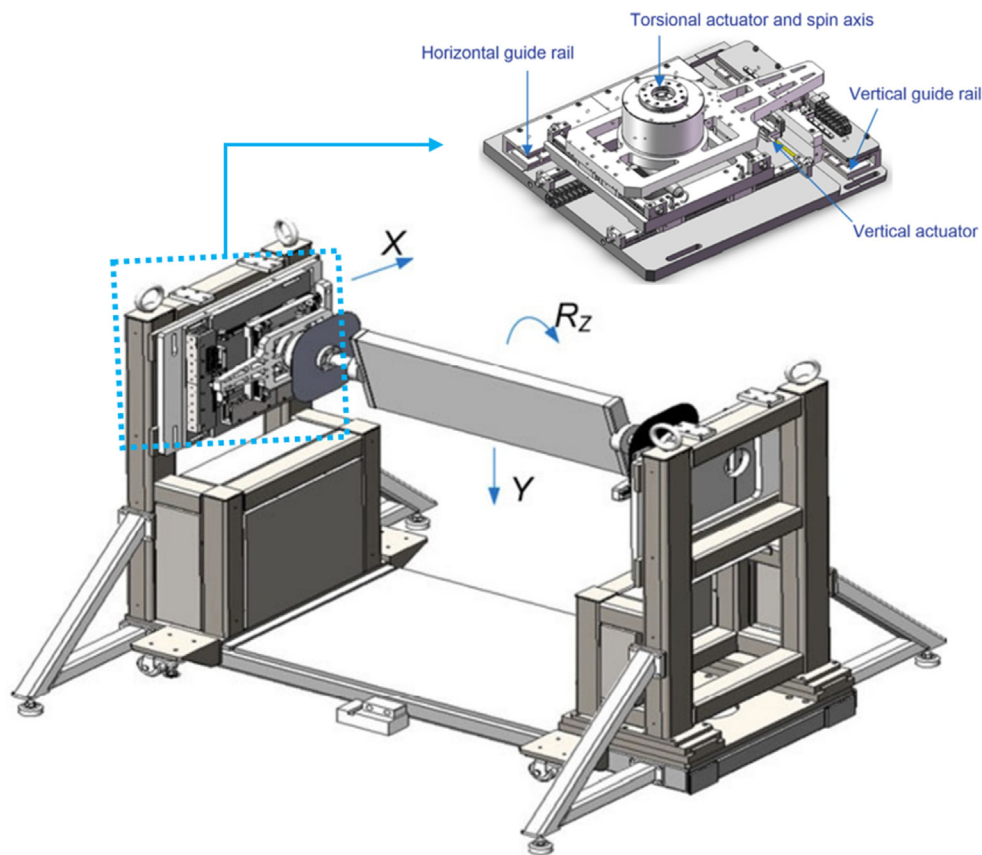where ρ is air density, U is incoming wind velocity, and B is width of the model.
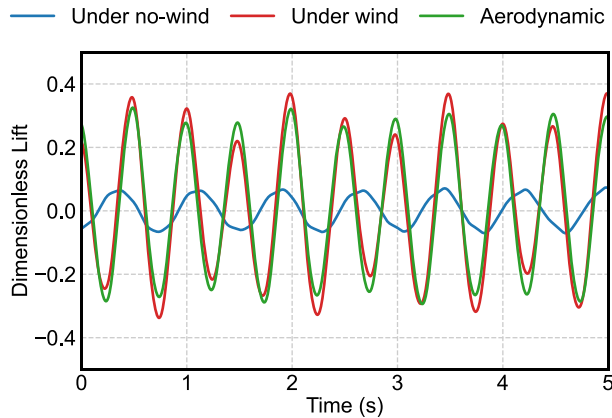

FIG. 2. Schematic diagram of forced motion device.

FIG. 4. Measured forces under wind/no wind and aerodynamic lift example.
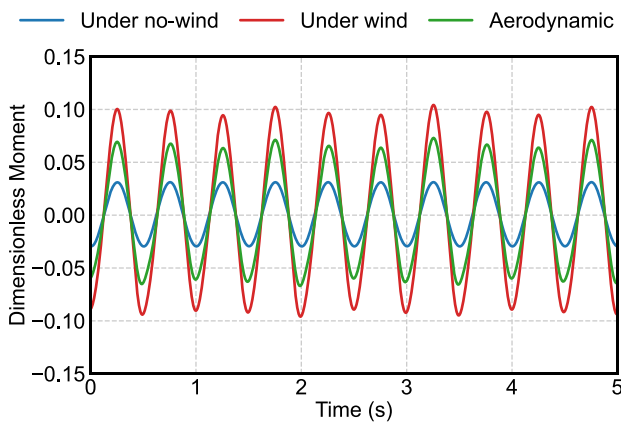

FIG. 5. Measured forces under wind/no wind and aerodynamic moment example.

Figures 4 and 5 show that a pair of dynamic forces time series measured by balances under wind condition, still air, respectively, and aerodynamic are also shown in following figures. "Under wind" line means the measured value by balances under a certain wind speed, and "aerodynamic" line means the calculation result by wind–nowind.

B. Dataset description

Vertical and torsional coupled motion is considered as research object in this work. The motion in vertical and torsional directions is harmonic, which is expressed as Eq. (2)

$$\alpha(t) = A \sin(\omega_\alpha t)(^\circ),$$
$$h(t) = r_A A \sin(\omega_h t)(\text{mm}),$$
$$(2)$$

where $\alpha(t)$ and $h(t)$ are torsional and vertical displacement time series, respectively; A is amplitude of oscillation; ω_α and ω_h are torsional and vertical circular frequency; and r_A is amplitude ratio between vertical and torsional.

The dataset in this work is organized by two dimensions called motion configuration and motion scale. Motion configuration is the normalized motion of quasi-plate, and motion scale is the time and

TABLE I. Aerodynamic motion-force dataset: forced motion configurations.

Configuration id	r_A	ω_α	ω_h	AoA
A	1.5	1.4 π	4 π	0
B	1.5	4 π	1.4 π	0
C	1.5	4 π	2.6 π	0
D	1.5	2.6 π	4 π	0
E	1	2.6 π	4 π	0
F	2	2.6 π	4 π	0
G	1.5	2.6 π	4 π	3

TABLE II. Aerodynamic motion-force dataset setting: forced motion scales.

Parameter	Value
Amplitude A	3,6,9,12,15,18,21,24
Wind speed(m/s) U	3,4,5,6,7,8,9,10

space scale of motion. Specifically, r_A, ω_α, and ω_h determine motion configuration. Motion space scale is influenced by A and timescale is affected by incoming wind speed. The whole dataset contains 7 motion configurations, as shown in Table I. Table II describes that each motion configuration has 8 wind speed scales and 8 amplitude scales. The total number of test cases is 448.

III. NONLINEAR AERODYNAMIC FORCE EQ. DISCOVERY METHODS

In this section, the model discovery method is described, which can derive governing equations from data. First, the mathematical background for equation discovery via sparse regression is given in Sec. III A. Section III B describes the group sparse regression strategy to consider dataset relationship on physical laws. Then, the setup of nonlinear aerodynamic expression discovery problem is discussed in Sec. III C. Section III D shows how to optimize hyper-parameters in regression process. Finally, a numerical validation is given in Sec. III E to prove the accuracy of algorithms.

A. Mathematics background of sparse identification

The nonlinear parameters of sparse identification methods are described to find equations from data. This method is inspired by sparse identification of nonlinear dynamical systems (SINDy) (Brunton et al., 2016). SINDy is a mathematical method for learning dynamics system via sparse regression. In this work, the sparse regression is used to find the simple and accurate semi-empirical expression via test or simulation data.

Consider a physical variate y determined by a couple of variate $X = [x_1, x_2, \ldots, x_n] \in \mathbb{R}$, which is defined by Eq. (3). The nonlinear mapping function f is the target to seek. It always can be rewritten by multivariate Taylor series in Eq. (4) and simplified as high-order multiple-term formula. This is the raw semi-empirical expression form of y, and $f_{x_{ki}}^{(n)}$ is the parameter, which is identified from data snapshot. However, physical system of interest always consists of a few terms. That is to say, when represented in the appropriate terms, there is a sense in which it is sparse. The key idea behind this sparse regression

method is that if one supplies a sufficient high-order set of Taylor series terms for representing f, then the simple and accuracy terms can be identified using sparse regression techniques and other terms can be ignored. The explicit steps are as follows:

$$y = f(x_1, x_2, \ldots, x_n), \tag{3}$$

$$y = f(x_{k1}, x_{k2}, \ldots, x_{kn}) + \sum_{i=1}^{n}(x_i - x_{ki})f'_{x_{ki}}(x_{k1}, x_{k2}, \ldots, x_{kn})$$
$$+ \frac{1}{2!}\sum_{i,j=1}^{n}(x_i - x_{ki})(x_j - x_{kj})f''_{x_{ij}}(x_{k1}, x_{k2}, \ldots, x_{kn}) + O^n. \tag{4}$$

First, a set of measurements of X and y are collected at a sequence of steps in time, $t_1, t_2, \ldots, t_m$. These measurements are concatenated into two matrices, the columns of which correspond to different variables and the rows of which correspond to the time steps

$$X = \begin{bmatrix} x_1(t_1) & x_2(t_1) & \cdots & x_n(t_1) \\ x_1(t_2) & x_2(t_2) & \cdots & x_n(t_2) \\ \vdots & \vdots & \ddots & \vdots \\ x_1(t_n) & x_2(t_n) & \ldots & x_n(t_n) \end{bmatrix}, \quad y = \begin{bmatrix} y(t_1) \\ y(t_2) \\ \vdots \\ y(t_n) \end{bmatrix}. \tag{5}$$

Next, Taylor series terms are used to expand the basis physical variables, which are written as follows:

$$\Phi(X) = \begin{bmatrix} \phi^0(X) & \phi^1(X) & \phi^2(X) & \ldots & \phi^n(X) \end{bmatrix}. \tag{6}$$

We note that Φ is the Taylor series expanded form of X and $\phi^i(X)$ corresponds to a ith-order polynomial of X. It is assumed that each component of f can be represented by a sparse linear combination of such functions. The regression solution can be used to be solved for the coefficients used in these linear combinations:

$$y = \Phi(X)\Xi. \tag{7}$$

To find Ξ, the optimization problem expressed by Eq. (8) is solved. The coefficients Ξ make Eq. (7) accuracy and sparse, which means most of the terms in Ξ are zero

$$\Xi = \min_{\Xi} \frac{1}{2}(y - \Phi(X)\Xi)^2 + \|\Xi\|_1, \tag{8}$$

which is a standard l_1 regularization regression problem. $\|\cdot\|_1$ is defined by $\|\mathbf{M}\|_1 = \sum_{i,j}|M_{ij}|$. Eq. (8) is solved by LASSO regression (Tibshirani, 1996). However, this method often leads to incorrect sparsity pattern (Su *et al.*, 2017). Brunton *et al.* (2016) proposed the sequential threshold least squares algorithm to solve Eq. (8). The algorithm does a loop between solving least squares problem for Ξ and removing candidate functions whose corresponding components are below the threshold δ. The loop will finish until all remained coefficients are larger than the threshold δ. The algorithm can be summarized as Algorithm 1.

B. Group sparse regression method

The standard sparse regression approach tries to learn the governing equations from each state variable independently. It does not take into account prior information one may possess regrading relationships between different cases. In this work, the aerodynamic forces of same motioned configurations with different frequency and amplitude are similar enough, which means their governing equations should include similar terms. In this subsection, a group sparse regression strategy is described, which ensures this hypothesis when seeking equations for nonlinear aerodynamic.

The group LASSO regression is presented by Yuan and Lin (2006). Classical LASSO method solves the standard l_1 regularization regression problem, which is expressed by Eq. (8) and penalizes the magnitude of Ξ individually. The group LASSO approach computes the penalty terms by bundling sets of related entries. Considering some similar cases, the coefficient of same term can be spliced into a vector $\Xi_1, \Xi_2, \ldots, \Xi_g$. The group LASSO solves the modified optimization problem as

$$\Xi = \min_{\Xi} \frac{1}{2}(y - \Phi(X)\Xi)^2 + \lambda \sum_{i=1}^{g} \|\Xi_i\|_1. \tag{9}$$

ALGORITHM 1. Aerodynamic semi-empirical expression of the sparse identification method.

	Input: $\mathbf{F} \in \mathbb{R}^{m \times 1}$, $\Phi(\mathbf{X}) \in \mathbb{R}^{m \times p}$, and $\delta > 0$
	Output: coefficients matrix $\Xi \in \mathbb{R}^{p \times 1}$
1	**while** *not converged* **do**
2	/∗ Solve a least squares problem ∗/
3	$\Xi \leftarrow \text{argmin}_{\Xi} \frac{1}{2}\|\mathbf{F} - \Phi(X)\Xi\|_2^2$;
4	/∗ Remove library terms with low contribution ∗/
5	**for** $i \leftarrow 1 \rightarrow p$ **do**
6	**if** $abs(\Xi_{(i,:)}) \text{¡} \delta$ **then**
7	Remove $\Xi_{(i,:)}$ and $\Phi(\mathbf{X})_{(:,i)}$
8	**end**
9	**end**
10	**end**

ALGORITHM 2 Aerodynamic semi-empirical expression group of the sparse identification method.

	Input: $\mathbf{F} \in \mathbb{R}^{m \times d}$, $\Phi(\mathbf{X}) \in \mathbb{R}^{m \times p}$, and $\delta > 0$
	Output: coefficient matrix $\Xi \in \mathbb{R}^{p \times d}$
1	**while** *not converged* **do**
2	/∗ Solve a least squares problem ∗/
3	**for** $j \leftarrow 1 \rightarrow d$ **do**
4	$\Xi \leftarrow \text{argmin}_{\Xi} \frac{1}{2}\|\mathbf{F} - \Phi(X)\Xi\|_2^2$;
5	**end**
6	/∗ Remove library terms with low contribution ∗/
7	**for** $i \leftarrow 1 \rightarrow p$ **do**
8	**if** $abs(\Xi_{(i,:)}) < \delta$ **then**
9	Remove $\Xi_{(i,:)}$ and $\Phi(\mathbf{X})_{(:,i)}$
10	**end**
11	**end**
12	**end**

When dataset has multiple cases, the group LASSO penalty tries to retain or remove each term as a group.

Group sparsity regularization is also used in SINDy framework (de Silva *et al.*, 2020) to learn unified physical law from similar cases. To enforce the condition that each governing equation should involve the same terms, the rows of Ξ as sets of variables are to be grouped together. The modified sequential threshold least squares with group sparse constraint have the following steps until convergence: (a) solve the standard least squares problem for each column of Ξ (for each test cases) and (b) remove the candidates, which have low relevance across most or all of the cases. The procedure is shown in Algorithm 2.

C. Aerodynamic force equation library

From the past research of aerodynamic forces, the lift L and moment M are related to motion $\mathbf{X}$, which contains vertical and torsional displacements h, α and their first-order derivative $\dot{h}, \dot{\alpha}$. The aerodynamic expression is written as Eq. (10). Third-order polynomial term $\Phi(X)$ combinations are used to represent Eq. (10) explicitly. The candidate terms are visualized in Fig. 6.

$$L = f(\alpha, \dot{\alpha}, h, \dot{h}), \quad M = g(\alpha, \dot{\alpha}, h, \dot{h}), \tag{10}$$

$$\Phi(\mathbf{X}) = \begin{bmatrix} \alpha & \dot{\alpha} & h & \dot{h} & \alpha^2 & \alpha\dot{\alpha} & \dots & \dot{h}^3 \end{bmatrix}. \tag{11}$$

Equation (11) consists of four first-order terms, ten second-order terms, and twenty third-order terms. However, third-order terms and first-order terms are not completely linearly independent, which is expressed as follows:

$$\frac{\alpha^3}{\alpha_0^3} + \frac{\alpha\dot{\alpha}^2}{\omega^2\alpha_0^3} = \sin(\omega t) = \frac{\alpha}{\alpha_0}. \tag{12}$$

That means that $\alpha\dot{\alpha}^2$; $\alpha^2\dot{\alpha}$; $h\dot{h}^2$; and $h^2\dot{h}$ can be expressed by the linear combination of α^3, α; $\dot{\alpha}^3, \dot{\alpha}$; h^3, h; and $\dot{h}^3, \dot{h}$, respectively. Therefore, these four third-order cross terms are removed from aerodynamic library in this study.

Note that motion library is the polynomials in $[\alpha, \dot{\alpha}, h, \dot{h}]$ up to third order. In most of practical cases, the plate will do simple harmonic motion in vertical and torsional degrees with same frequency, like flutter. However, this motion should not be used to identified nonlinear function f, g correctly. The reason is that a sinusoidal function is the linear combination of other two sinusoidal functions with the same frequency. The same frequency motion data will lead a linear

dependence library and a wrong sparse model. As Fig. 6 shows, α and h motions have different frequencies, which guarantee each candidates in library is linear independent.

Without prior knowledge for physical model finding, key aerodynamic terms are selected from Eq. (11) by the sequential threshold least squares algorithm. In traditional linear theory, aerodynamic force is a linear function of motion and speed (Theodorsen and Mutchler, 1935; Scanlan and Tomko, 1971). This is the aerodynamic expression prior knowledge, which should be considered in this work. That is to say, linear terms ($\alpha, \dot{\alpha}, h, \dot{h}$) are kept constantly in Eq. (11) and other nonlinear terms are selected by sparse regression.

D. Hyper-parameter optimization

This part wants to simplify the Taylor series of Eq. (10) and find several key terms from candidate library in Eq. (11) using the sparse regression method. Each test case will get an aerodynamic-motion time series and find a sparse expression. The procedure is summarized in Algorithm 1. Absolute value of coefficient measures the importance of a candidate. Convergence is attained when no terms of Ξ are removed. The hyper-parameter δ controls the sparsity of Ξ. The expression will remain fewer terms with δ increasing.

δ in Algorithm 1 and 2 is the key factor to determine whether aerodynamic model is sparse and correct or not. In previous machine learning algorithm, hyper-parameters are decided by regression metrics, like R^2 score. Specifically, iterative training algorithm is used to try different values of hyper-parameter until the regression metrics reaching to an optimized value (like $R^2 > 0.99$). However, the unique characteristic of this case is that, on the one hand, accuracy is not the only important metric, and the balance of sparsity and accuracy are also important as well; on the other hand, it is that traditional metrics cannot represent whether nonlinear model is suitable or not.

Here, it is an example to explain this special characteristic specifically. An aerodynamic force-motion dataset is built by wind tunnel test, with two degrees of freedom (2DOF) harmonic motion, which is expressed as follows:

$$\begin{aligned} \alpha(t) &= 24° \sin(2 \times 2\pi t), \\ h(t) &= 36\text{mm} \sin(1.3 \times 2\pi t), \end{aligned} \tag{13}$$

which is the flat center point motion function. The aerodynamic forces are measured by balances and are shown as the gray line in Fig. 7.
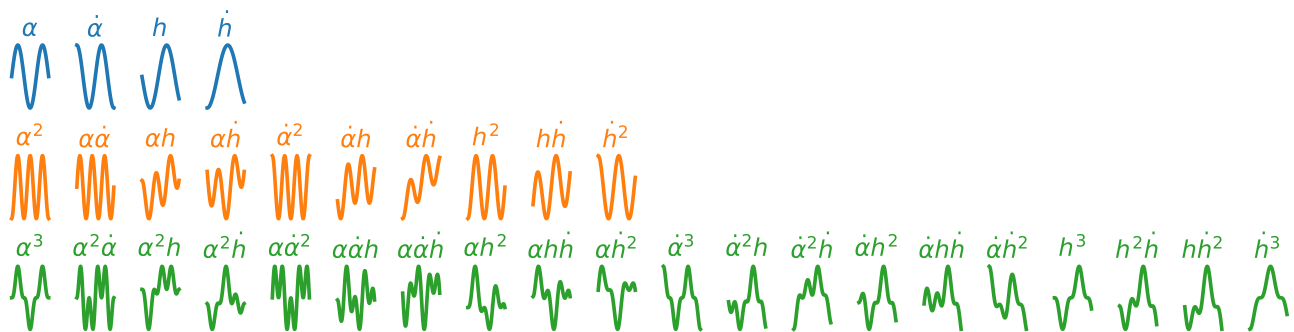

FIG. 6. Visualizations of nonlinear library functions corresponding to the harmonic motioned object aerodynamic force.
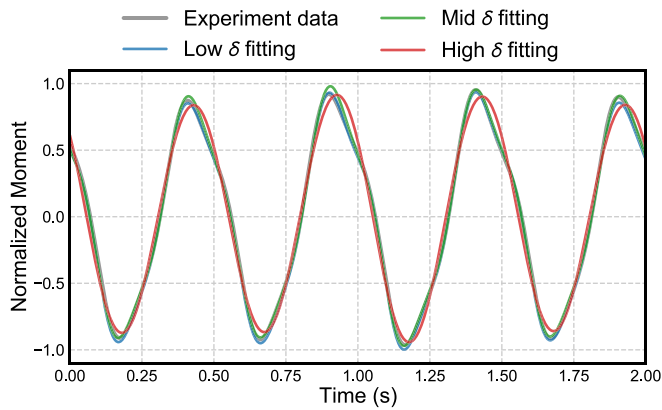
FIG. 7. An example of experiment data aerodynamic moment and sparse identification result with different δ.
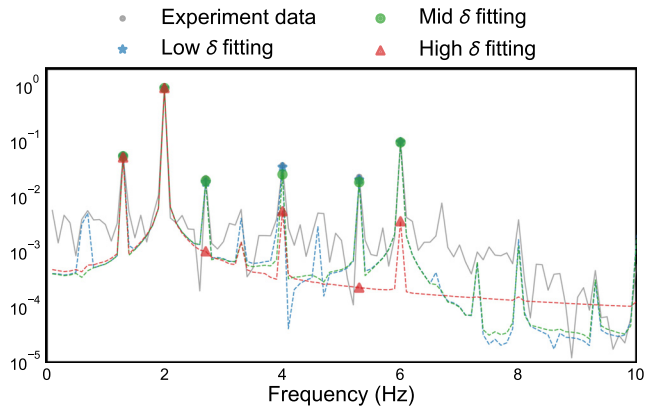

FIG. 8. An example of experiment data aerodynamic moment and sparse identification result with different δ in frequency domain.

Algorithm 1 is used to find the aerodynamic force equation from this sample with different δ. The prediction moment from different selected equations is shown in Fig. 7. Three different δ are compared with high, middle, and low values. The testing cases are described specifically in Table III. Generally, sparse regression model with high δ will filter out most of nonlinear aerodynamic terms and only keep the most effective terms. Theoretically, the equation combined by fewer terms has lower accuracy. Lower δ leads to the opposite situation. However, three different δ almost have the same model rebuilding accuracy in Fig. 7, which is also shown in Table III that R^2 score cannot stand for whether selected model is a suitable one for aerodynamic physical law.

The most important for a nonlinear equation is whether it can represent the nonlinear part of dynamic system, not just the time series fitting accuracy. Linear equation also can rebuild the system in time domain (like previous example case high). Frequency-domain rebuilding performance is another good metric to ensure the system nonlinearity. Several aerodynamic research proves that nonlinear aerodynamic force has multi-frequency effect, which means simple harmonic motion flat has high-order frequency components aerodynamic forces (Diana *et al.*, 2004; Falco *et al.*, 1992; and Liu *et al.*, 2022). Simple harmonic motion is concentrated on only two basic frequencies, and aerodynamic force spectrum has several peaks only on the multiples of motion basic frequency. Figure 8 shows that the spectrum of four curves in Fig. 7 and spectrum peaks on frequency domain

stand for system nonlinearity. The difference between three identified models is obvious in frequency domain.

The ideal model should rebuild system very accurately on the key frequencies and have few nonlinear terms as possible. The aerodynamic system rebuilding metrics are defined as the mean squared error between experimental data and model rebuilding on top k largest frequencies

$$Loss = \frac{1}{k}\sum_{i=1}^{k}\frac{(Y_i - \hat{Y}_i)^2}{Y_i^2}, \tag{14}$$

where Y_i is the experimental force frequency value on ith key frequency and $\hat{Y}_i$ means the model rebuilding value. With hyperparameter δ increasing, $Loss$ of sparse model increases and nonlinear terms number decreases.

E. Numerical verification

A numerical example is described in this subsection to show the candidate terms of equations and sparse regression accuracy. A simulated nonlinear aerodynamic equation is designed to make some virtual aerodynamic motion-force data. Least-squares, sparse regression, and group sparse regression methods are used to rebuild this equation from data.

A simulated nonlinear aerodynamic equation is defined as Eq. (15). For algorithm testing, Eq. (15) has four linear terms, as flutter derivative theory, and two nonlinear terms chosen arbitrary

$$F = H_1 h + H_2 \dot{h} + A_1 \alpha + A_2 \dot{\alpha} + N_1 h \dot{h} \alpha + N_2 \alpha^2 h + \mathcal{N}(0, 0.5), \tag{15}$$

where F is aerodynamic force; h, α are vertical and torsional displacement, respectively; $\dot{h}, \dot{\alpha}$ are vertical and torsional velocity, respectively; H_1, H_2, A_1, A_2 are coefficients for linear terms; and N_1, N_2 are coefficients for nonlinear terms. Furthermore, an additive Gaussian noise of the form $\mathcal{N}(0, 0.5)$ is added into simulation.

Then, as Eq. (16) shows, a two-dimension harmonic motion is designed to build aerodynamic motion-force datasets. There are two pre-defined parameter groups (Table IV) that are used to simulate nonlinear aerodynamic force

TABLE III. The rebuilding performance of sparse regression model with different δ in sample aerodynamic-motion dataset.

Case	δ	Linear terms	Nonlinear terms	R^2 score	Description
High	1	4	0	0.985	Linear model
Middle	0.01	4	2	0.993	Sparse nonlinear model
Low	0.0001	4	10	0.996	Dense nonlinear model

TABLE IV. Virtual aerodynamic equation parameters.

Group	A_1	A_2	H_1	H_2	N_1	N_2
1	0.9	0.1	-0.4	0.03	0.05	0.3
2	0.1	0.3	-0.1	0.2	0.5	0.8

TABLE V. Numerical aerodynamic sample parameter identification results.

Aerodynamic term	Group 1		Group 2	
	Ground truth	Prediction	Ground truth	Prediction
α	0.90	0.88	0.10	0.10
$\dot{\alpha}$	0.10	0.10	0.30	0.30
h	-0.40	-0.39	-0.10	-0.07
$\dot{h}$	0.03	0.03	0.20	0.20
$\alpha^2 h$	0.30	0.27	0.80	0.75
$\alpha h \dot{h}$	0.05	0.05	0.50	0.50
Other terms	All zero	All zero	All zero	All zero
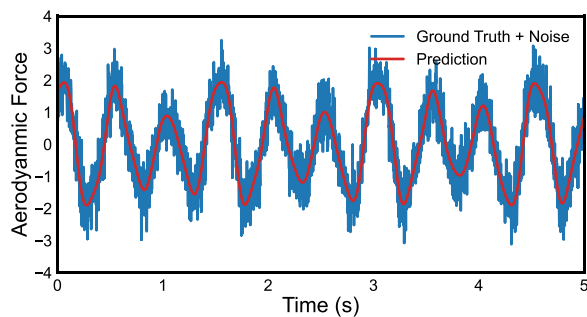
FIG. 9. Aerodynamic force of parameter group 1 sparse regression result and simulation data.

$$\alpha(t) = \sin(2 \times 2\pi t),$$
$$h(t) = \sin(1.3 \times 2\pi t). \tag{16}$$

The sparse regression method is used to find the effective terms by virtual aerodynamic force-motion data. The original aerodynamic equations can be written as

$$F = \Phi(\mathbf{X})\Xi, \tag{17}$$

where $\Phi(\mathbf{X})$ consists the first three-order polynomial terms of $[\alpha, \dot{\alpha}, h, \dot{h}]$, as Eq. (11).

The result of regression is shown in Table V and Figs. 9 and 10. It can be clearly seen that the sparse regression method can find the accuracy terms of aerodynamic equation even with Gaussian noise.

IV. IDENTIFICATION RESULTS IN DIFFERENT CASES

In this section, nonlinear terms present in the aerodynamic governing equations are identified by the sparse identification method.
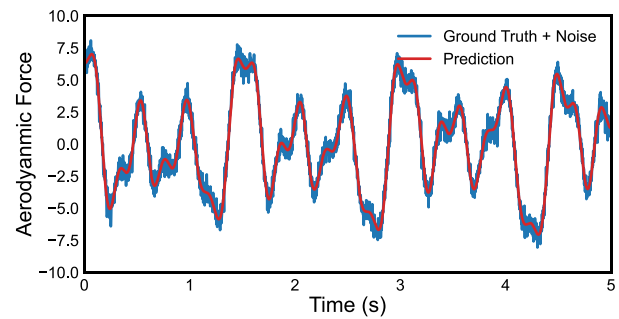

FIG. 10. Aerodynamic force of parameter group 2 sparse regression result and simulation data.

ALGORITHM 3. Sparse regression hyper-parameter δ optimization.

Input: $\mathbf{F} \in \mathbb{R}^{m \times 1}$, $\Phi(\mathbf{X}) \in \mathbb{R}^{m \times p}$, $Loss_{limit}$, k, and $d\delta$
Output: δ
1   $\delta \leftarrow 0$;
2   **while** $Loss <= Loss_{limit}$ **do**
3 | $\Xi \leftarrow$ Sparse regression(δ); //Calculate Ξ by using Algorithm 1
4 | $\hat{\mathbf{F}} \leftarrow \Phi(\mathbf{X})\Xi$;//Rebuild system
5 | $S(\mathbf{F}) \leftarrow fft(\mathbf{F})$;
6 | $S(\mathbf{F})_{key}$, idx $\leftarrow k$ largest $(S(\mathbf{F}))$; //Estimate values and indexes of k largest elements from $S(\mathbf{F})$
7 | $S(\hat{\mathbf{F}})_{key} \leftarrow S(\hat{\mathbf{F}})($ idx $)$; //Get values from $S(\hat{\mathbf{F}})$ at same key frequency
8 | $Loss \leftarrow \frac{1}{k}\left(S(\hat{\mathbf{F}})_{key} - S(\mathbf{F})_{key}\right)^2$;
9 | $\delta = \delta + d\delta$;
10 **end**

There are several aerodynamic-motion datasets, which have different motion configurations, incoming wind speeds, and motion amplitudes. Dataset is measured by forced motion wind tunnel test, which is described in Sec. II. The sparse model is trained on each test case. Hyper-parameter δ is optimized by Algorithm 3. That means this model does not keep any terms which coefficient is lower than δ. The parameter δ is chosen to rebuild the system, while being restrictive enough to prevent widespread over-fitting.

A. Sparse aerodynamic parameter space in a certain cyclical motion

First, a pair of cyclical motion and aerodynamic force dataset is taken as an example to show how nonlinear aerodynamic function becomes sparse through the proposed identification method. The motion-force sample is shown in Fig. 11, which is measured from a quasi-flat plate moved Eq. (13) under 10 m/s wind speed.

As shown in Fig. 11, motion on vertical and torsional DOF has different frequencies. However, force on vertical and torsional DOF has same basic frequencies, which is same as torsional motion frequency. The linear part of 2DOF harmonic motion aerodynamic force is mainly affected by torsional motion. It is demonstrated more clearly
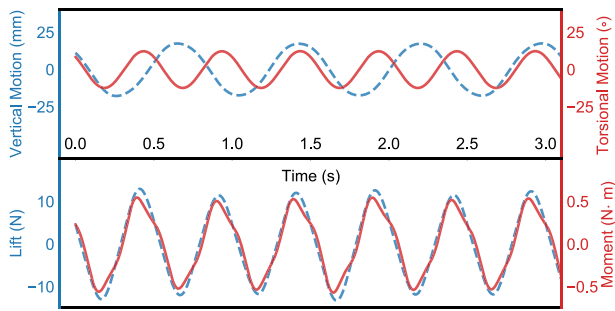
FIG. 11. A motion-force dataset visualization in time domain: Upper is motion and lower is Aerodynamic forces; red solid line stands for torsional motion and force; blue dashed line stands for vertical motion and force.
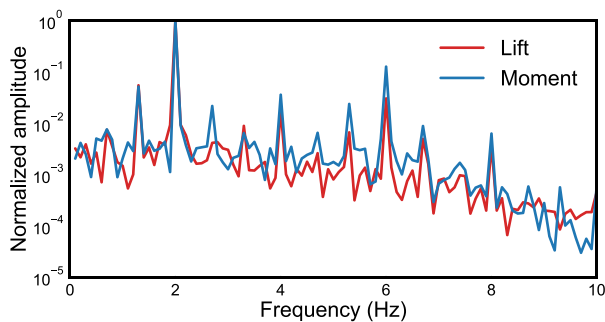

FIG. 12. A motion-force pair visualization in frequency domain: Red solid line stands for moment; blue dashed solid stands for lift.

in frequency domain (Fig. 12). There is almost no high-order harmonics in aerodynamic lift, which agrees with Liu *et al.* (2022). In Fig. 12, there is a high-order peak on 6 Hz, which is 3 times of torsional vibration frequency. This work mainly discusses the high-order terms, which could stand for nonlinear aerodynamic moment.

The sparse identification method is used to fit this motion-force sample and find the accurate nonlinear parameter. Figure 13 shows

how the Algorithm 1 selects the nonlinear parameters during δ growing. The nonlinear library has 30 terms when only considering up to the first three orders. Because of the spectral characteristics of aerodynamic moment, higher order more than 3 is not involved in this case. Figure 13 shows nonlinear parameter selection result and model rebuilding accuracy in linear and nonlinear part with five different δ values. Model rebuilding accuracy is the related error between ground truth and sparse expression rebuild result in frequency domain. Linear rebuilding performance does not depend on how much nonlinear parameter is selected. Meanwhile, nonlinear rebuilding performance slowly decreases with increasing δ and quantity of effective nonlinear candidates decreasing. It clearly shows that there is an optimal δ with acceptable accuracy can choose the fewest nonlinear candidates.

For this case, $\dot{\alpha}^3$ is chosen by the sparse regression method to stand for the nonlinear relationship between aerodynamic moment and motion. In this case, a concise expression of nonlinear aerodynamic can be found from data.

The sparse regression method is used to find the balance of rebuilding performance and simplicity. It has to sacrifice some "fitting score" of model. It clearly shows that nonlinear terms could dominate this nonlinear relationship.

B. Nonlinear aerodynamic parameters in different motion scales

This section discuss that how motion scale influences the nonlinear aerodynamic parameters. Specifically, the dataset of motion configuration A involves 8 amplitude and 8 wind speeds. Some aerodynamic force samples are shown in Figs. 14 and 15. The group sparse regression method is used to find general aerodynamic equation from these 64 motion-force time series.

Figure 16 summarizes the result of aerodynamic parameters identified by the group sparse regression method. This is a new visualization method for three-dimensional sparse regression. In this case, each parameter has three dimensions called amplitude, wind speed, and term name. So, how parameter of each terms changes on amplitude–wind speed axis is shown in Fig. 16. Each term's parameter on different test cases is represented by a heatmap. If the term is inactive on all test cases, the term name is gray and heatmap becomes transparent.
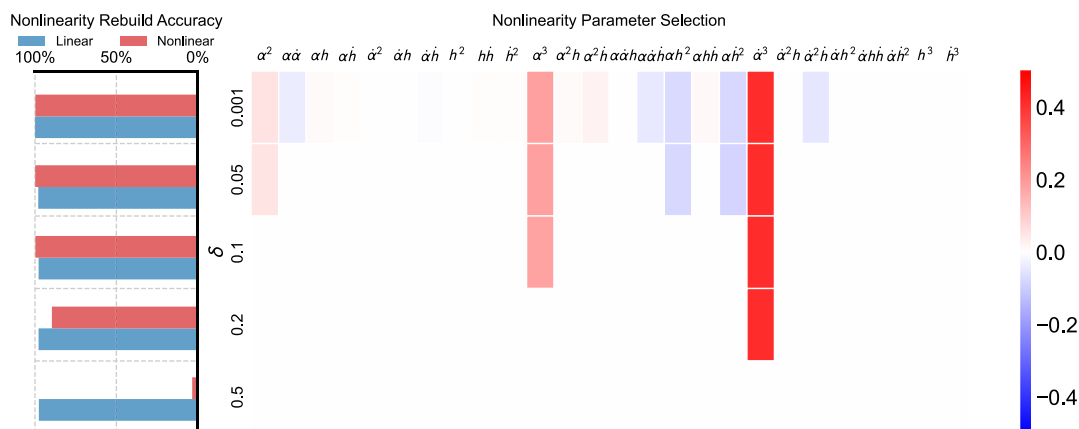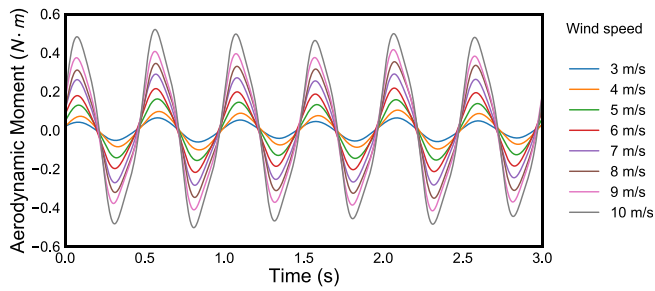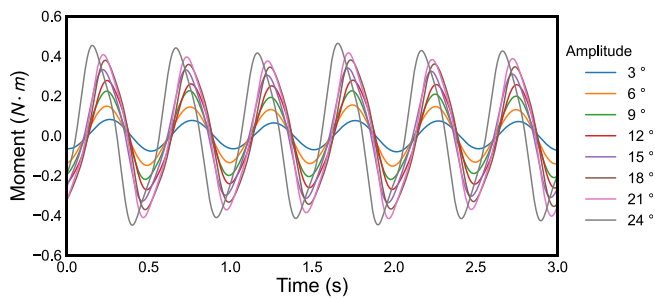

FIG. 13. How the sparse model select nonlinear parameters during δ growing, and its nonlinearity rebuild accuracy.

FIG. 14. The visualization of aerodynamic force under motion configuration: $\alpha(t) = 18°\sin(4\pi t)$; $h(t) = 27\text{mm}\sin(2.6\pi t)$ (wind speed ranges from 3 to 10 m/s).


FIG. 15. The visualization of aerodynamic force under motion configuration: $\alpha(t) = A°\sin(4\pi t)$; $h(t) = 1.5A\sin(2.6\pi t)$ (wind speed is 10 m/s; amplitude A ranges from 3 to 24).

In Fig. 16, $\alpha\dot{\alpha}$, α^3, and $\dot{\alpha}^3$ are effective on motion configuration A dataset. $\alpha\dot{\alpha}$ and α^3 are blue in heatmap, which means those coefficients are negative. Otherwise, the coefficients of $\dot{\alpha}^3$ are positive for large amplitude and large wind speed testing cases.

Then, Figs. 17 and 18 show the comparison between wind tunnel test and three nonlinear terms of sparse model in time domain and frequency domain, respectively. Intuitively, sparse model fits the data well. To calculate the quantitative rebuilding performance of aerodynamic sparse model, two metrics are introduced. First, one is R^2 score
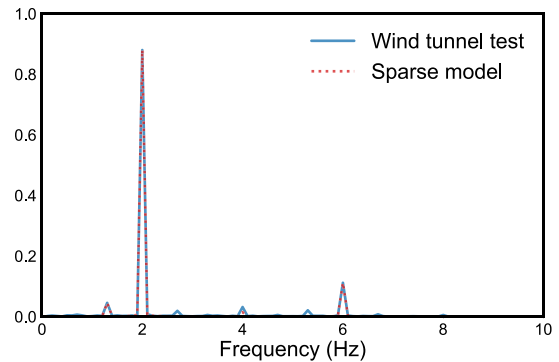

FIG. 17. The comparison between wind tunnel test result and sparse model in time domain; motion: $h(t) = 36\sin(2.6\pi t)$ mm, $\alpha(t) = 24\sin(4\pi t)°$; wind speed: 10 m/s.
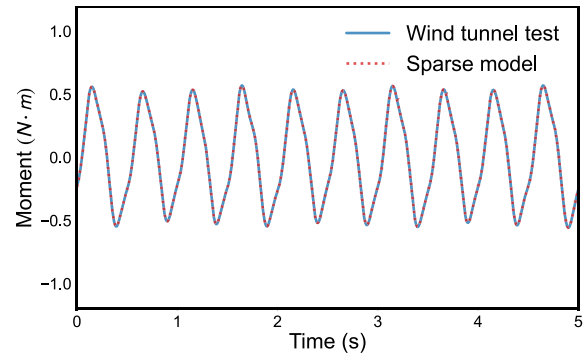
FIG. 18. The comparison between wind tunnel test result and sparse model in frequency domain; motion: $h(t) = 36\text{mm}\sin(2.6\pi t)$, $\alpha(t) = 24°\sin(4\pi t)$; wind speed: 10 m/s.

for time domain, and second one is main frequency-weighted accuracy (MFWA) for frequency domain, which is a new metric to show how aerodynamic model performs in several key frequencies only and ignores the others, as expressed in Eq. (18).
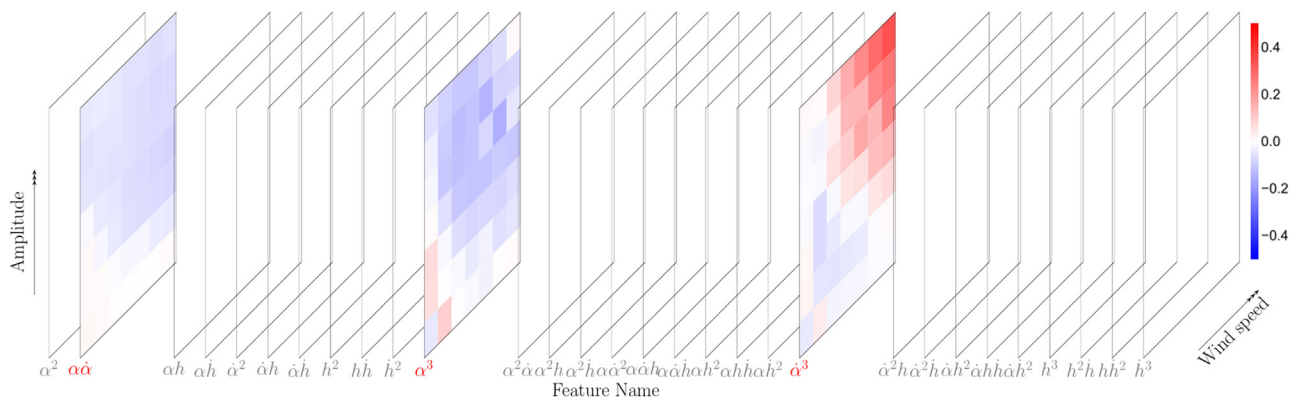
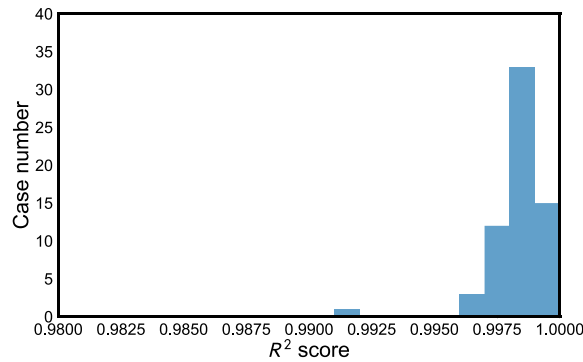FIG. 16. The multi-layer heatmap of group sparse regression result; training set: motion configuration D.

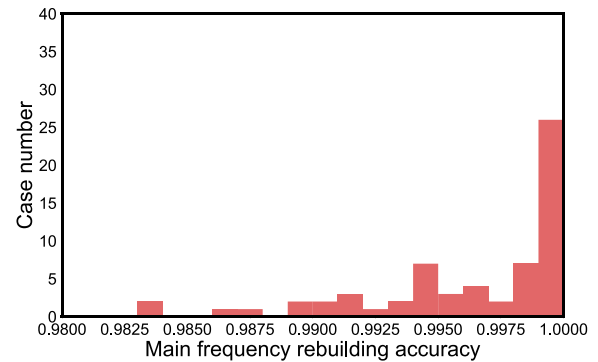**FIG. 19.** The histogram of sparse model R^2 score; training set: motion configuration A.

FIG. 20. The histogram of sparse model main frequency rebuilding accuracy; training set: motion configuration A.

$$\text{MFWA} = \sum_{i=1}^{n} \frac{\hat{f}_i \ f_i}{\sum \hat{f}_i \hat{f}_i}, \tag{18}$$

where n is the number of main frequency, f_i is the model predicting amplitude on ith key frequency, and $\hat{f}_i$ is the test data amplitude on ith key frequency. In this case, the key frequency of aerodynamic moment is considered as 2, 4, and 6 Hz.

Based on two quantitative metrics, how the three nonlinear terms of aerodynamic sparse model perform in 64 test cases of motion configuration A, which is shown in Figs. 19 and 20. The accuracy on time and frequency domain are all larger than 0.98. So, it proves that $\alpha\dot{\alpha}$, α^3, and $\dot{\alpha}^3$ can represent the 2DOF quasi-plate aerodynamic force.

C. The stability of sparse regression results under different conditions

Whether the effective aerodynamic nonlinear terms are same in different motion configurations is discussed in this subsection. The group sparse regression method is used to identify the effective terms on seven motion configuration datasets. The results are compared in three different motion configuration types, which involved amplitude ratio r_A, frequency ratio ω_α/ω_h, and angle of attack.

1. Amplitude ratio

First, motion configurations D, E, and F are considered to discuss whether amplitude ratios between vertical and torsional affect the sparse regression result. The only difference between these three configurations is amplitude ratio r_A. The group sparse regression method is used to find the effective nonlinear terms. The results are shown in Figs. 21–23.

Obviously, the effective nonlinear terms are kept stable when amplitude ratio is changing. The coefficients change rule during wind speed, and amplitude changing is also similar in these three cases. At large-amplitude range, $\alpha\dot{\alpha}$ and α^3 provide negative contributions for aerodynamic moment and the coefficients decrease gradually with the wind speed. The coefficients of heatmap of $\dot{\alpha}^3$ are diagonally distributed. In the case of large wind speed and large amplitude, which makes a positive contribution, while in the case of small wind speed and small amplitude, it makes a negative contribution.

2. Frequency ratio

Frequency of vertical and torsional motion is also significant for aerodynamic system. Motion configurations A–D are used to discuss how frequency ratios influence the effective nonlinear terms of aerodynamic. These test cases are in same condition, but vertical frequency ω_h and torsional frequency ω_α are different. Figures 24–27 show the
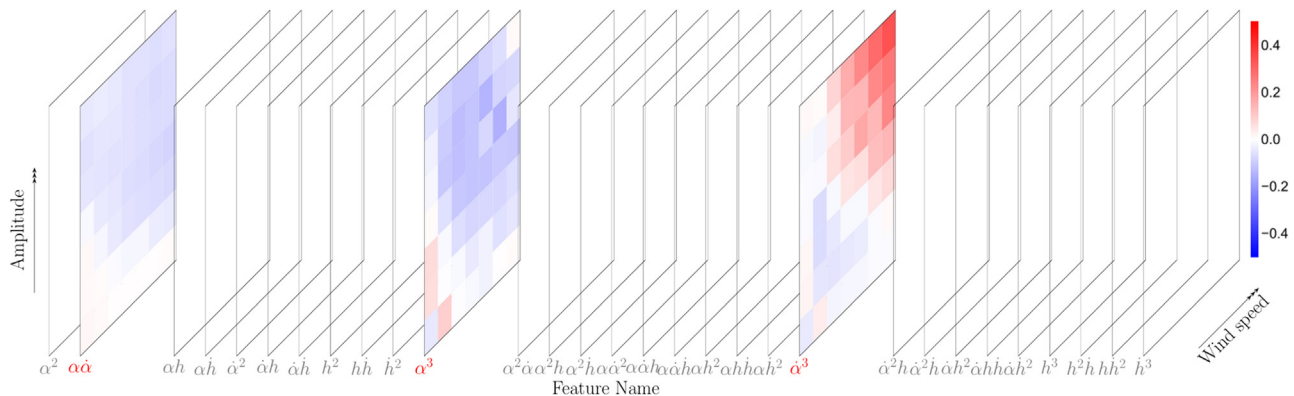

FIG. 21. The multi-layer heatmap result of motion configuration D: $\omega_h = 2.6\pi$, $\omega_\alpha = 4\pi$, $r_A = 1.5$, and AoA $= 0°$.
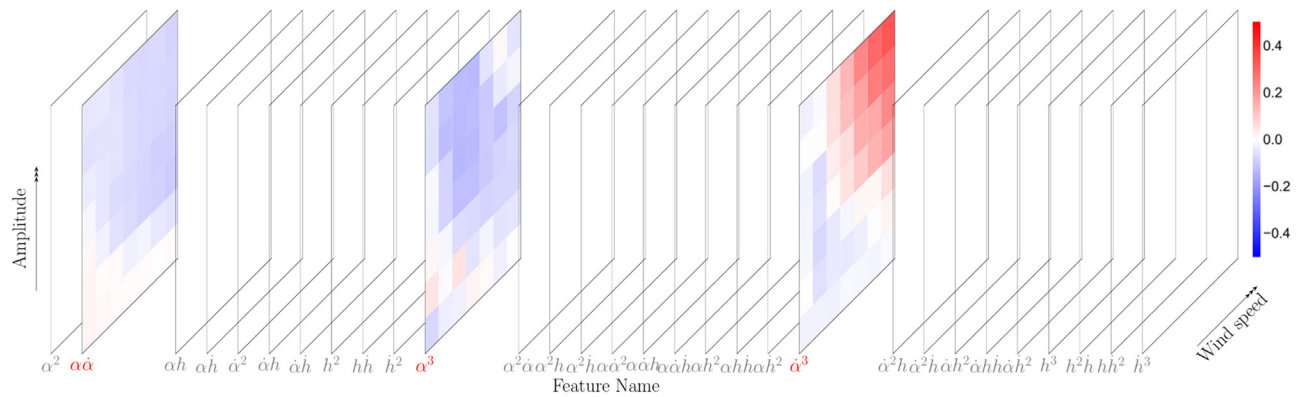
FIG. 22. The multi-layer heatmap result of motion configuration E: $\omega_h = 2.6\pi$, $\omega_\alpha = 4\pi$, $r_A = 1$, and AoA $= 0°$.
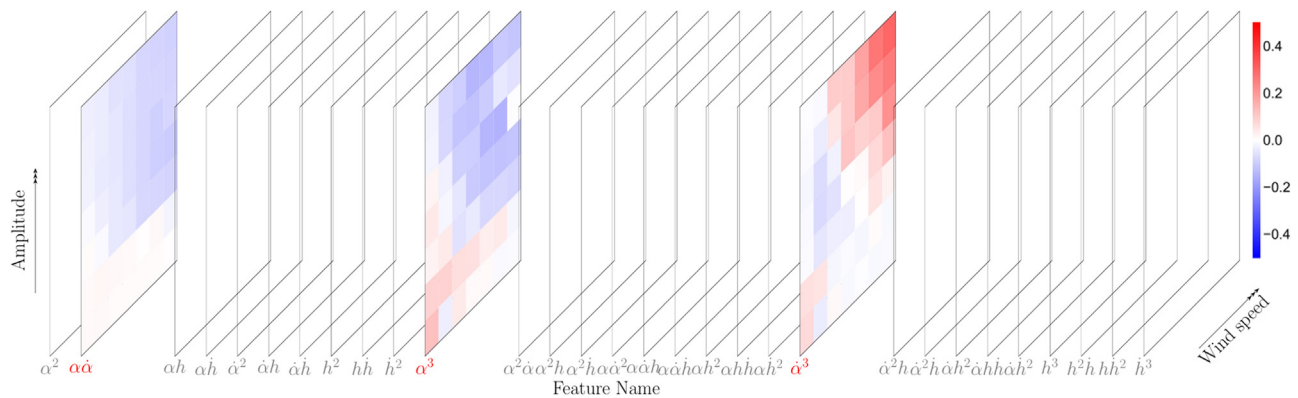

FIG. 23. The multi-layer heatmap result of motion configuration F: $\omega_h = 2.6\pi$, $\omega_\alpha = 4\pi$, $r_A = 2$, and AoA $= 0°$.

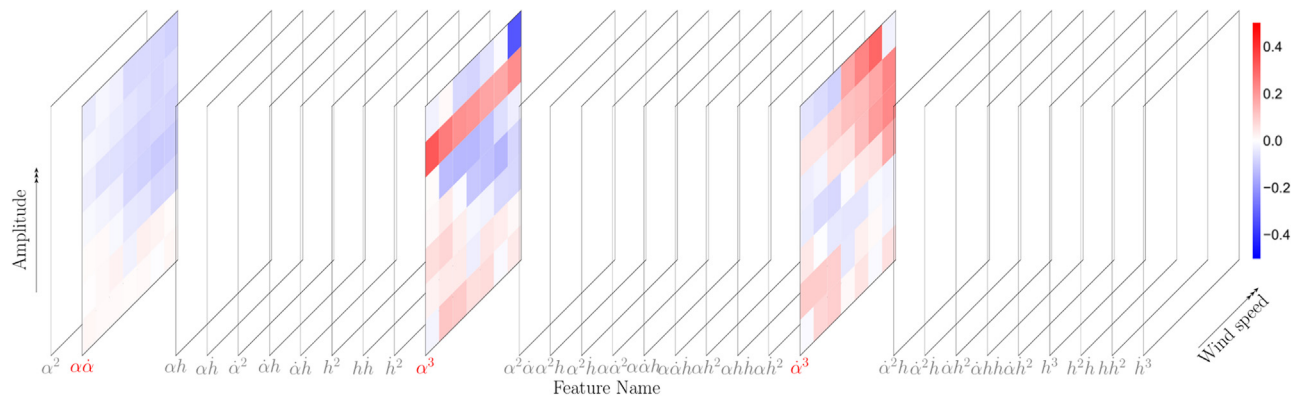**FIG. 24.** The multi-layer heatmap result of motion configuration A: $\omega_h = 1.4\pi$, $\omega_\alpha = 4\pi$, $r_A = 1.5$, and AoA $= 0°$.

sparse identification results of nonlinear aerodynamic parameters change $\omega_h : \omega_\alpha$ from low to high.

Obviously, $\alpha\dot{\alpha}$, α^3, and $\dot{\alpha}$ are also the active nonlinear aerodynamic terms in these motion configurations. Amplitude ratios do not change the distribution of coefficient values in amplitude–wind speed

axis. When vertical frequency ω_h rises relative to torsional frequency ω_α, coefficients of α^3 turn from negative to positive, especially in motion configuration B. The diagram distribution of $\dot{\alpha}^3$ seems like moving to low amplitude and low wind speed direction. The positive part in α^3 heatmap becomes larger for rising ω_h.
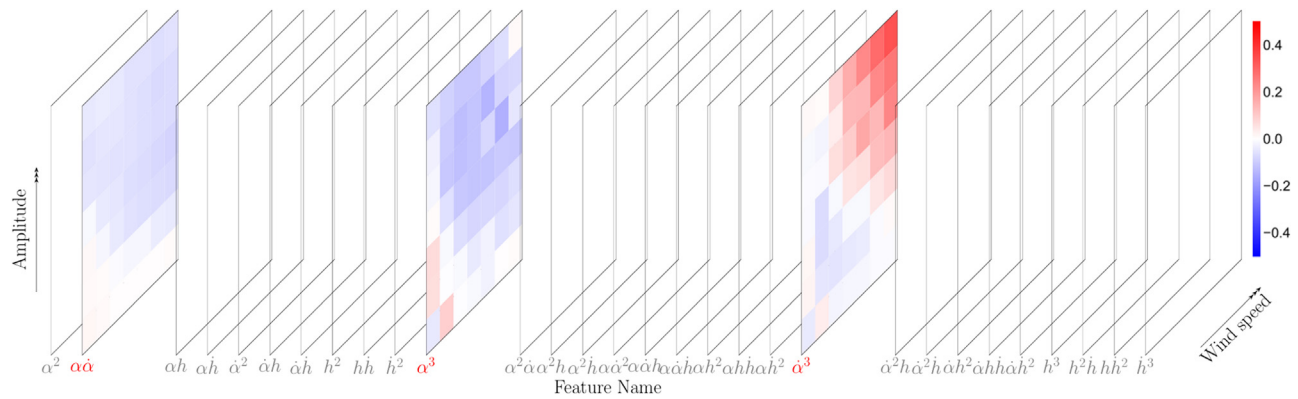
FIG. 25. The multi-layer heatmap result of motion configuration D: $\omega_h = 2.6\pi$, $\omega_\alpha = 4\pi$, $r_A = 1.5$, and AoA $= 0°$.

FIG. 26. The multi-layer heatmap result of motion configuration C: $\omega_h = 4\pi$, $\omega_\alpha = 2.6\pi$, $r_A = 1.5$, and AoA $= 0°$.

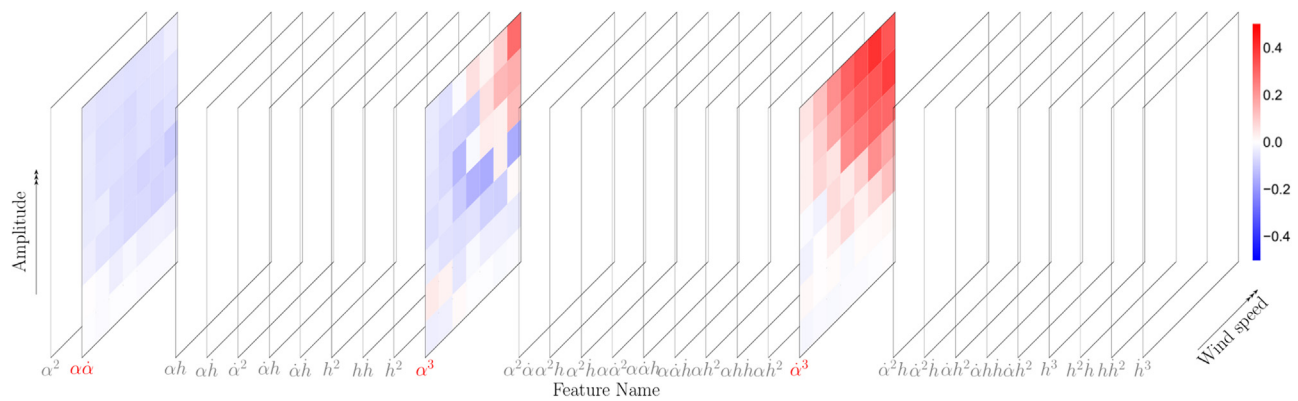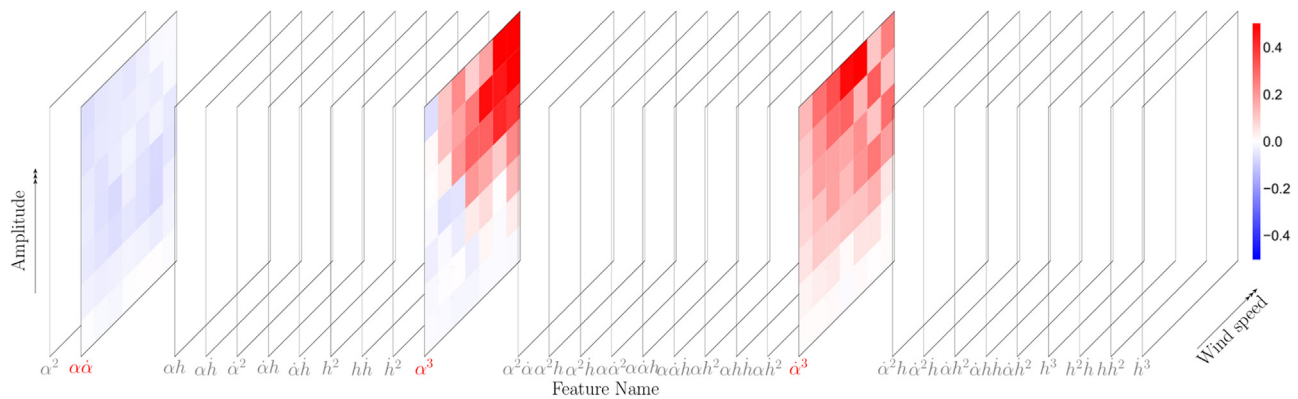**FIG. 27.** The multi-layer heatmap result of motion configuration B: $\omega_h = 4\pi$, $\omega_\alpha = 1.4\pi$, $r_A = 1.5$, and AoA $= 0°$.

3. Angle of attack

Generally, large angle-of-attack (AoA) aerodynamic system is considered "more nonlinear" than small angle of attack one. In this subsection, this problem is discussed in the view of nonlinear terms of sparse regression. Motion configuration G is compared with D, which is only different in AoA. Figure 28 shows the sparse regression result of motion configuration G. Comparison between Figs. 28 and 16, the weight of $\alpha\dot{\alpha}$ is larger. Compared with motion configuration D, non-zero and nonlinear parameters occur in lower amplitude at this case, especially in $\dot{\alpha}^3$ layer.
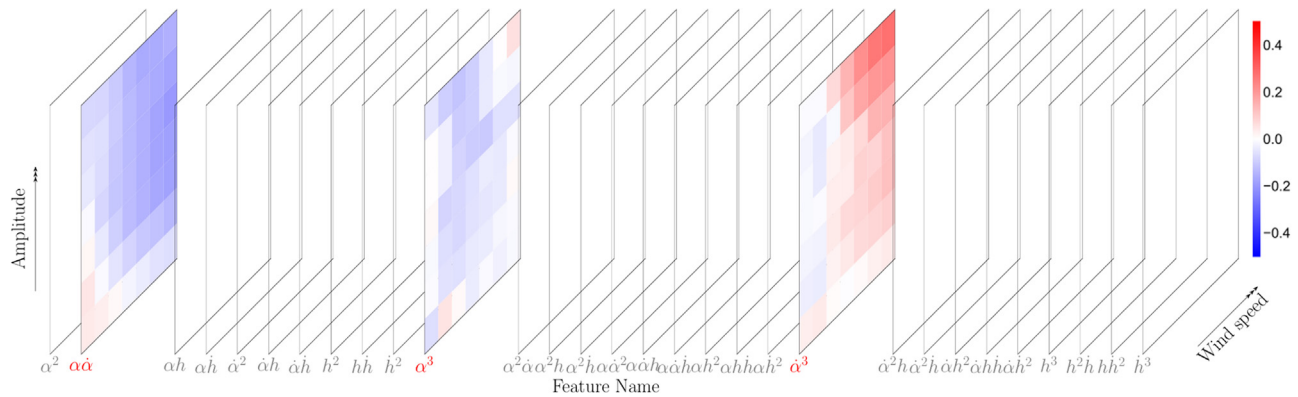
FIG. 28. The multi-layer heatmap result of motion configuration G: $\omega_h = 4\pi, \omega_\alpha = 1.4\pi, r_A = 1.5$, and AoA = 3°.

D. Result summary

This section discusses that the aerodynamic nonlinear equations of sparse regression results in different motion configurations. The results show that amplitude ratio, vertical and torsional frequency, and AoA do not change the effective nonlinear terms. The aerodynamic moment of vertical and torsional coupled harmonic motion quasi-plate can be expressed as

$$M = \frac{1}{2}\rho U^2 B^2 \left[KA_1^* \frac{\dot{h}}{U} + KA_2^* \frac{B\dot{\alpha}}{U} + K^2 A_3^* \alpha + K^2 A_4^* \frac{h}{B} \right.$$
$$\left. + K^3 N_1^* \frac{B}{U}\alpha\dot{\alpha} + K^6 N_2^* \alpha^3 + K^3 N_3^* \frac{B^3}{U^3}\dot{\alpha}^3 \right], \qquad (19)$$

where $K = \omega B/U$ denotes reduced frequency; A_i^* is the linear flutter derivatives and N_i^* is the nonlinear derivatives; U is wind speed; and B is the width of plate.

For a quasi-flat plate with two degrees of freedom harmonic motion, the amplitude ratio, frequency ratio, and angle of attack will not change the nonlinear effective term, but will change the distribution of its coefficients.

V. CONCLUSION

In this paper, a nonlinear aerodynamic model for form-finding method based on group sparse identification method is proposed, which can intelligently build nonlinear aerodynamic force expression from experimental data. The algorithm balances the simplicity of the model and the fitting accuracy, and selects the control parameter terms in the nonlinear aerodynamic equation. In order to quantify the algorithm fitting performance on aerodynamic force, the main frequency weighted accuracy is proposed as a new metric. Based on this metric, a hyper-parameter optimization method is created to improve the performance of sparse regression in this paper.

The effectiveness of the algorithm is verified by taking the quasi-plate section of the vertical–torsional coupling simple harmonic vibration as an example. It is found that $\alpha\dot{\alpha}, \alpha^3, \dot{\alpha}^3$ are the nonlinear effective parameters of the aerodynamic force of the quasi-flat plate in vertical–torsional coupled vibration and its coefficient changes uniformly with the amplitude and wind speed. The effective aerodynamic nonlinear terms are same when amplitude ratio, frequency ratio, and angle of attack are changing.

A concise nonlinear aerodynamic equation makes the physical explanation possible. If the quantity of model's parameters is large, the coefficient analysis could not be done like flutter derivatives. In the future work, how the nonlinear parameter changes and what does it meaning is on the list. It will be helpful to understand nonlinear aerodynamic deeply.

AUTHOR DECLARATIONS

Conflict of Interest

The authors have no conflicts to disclose.

Author Contributions

Teng Ma: Conceptualization (lead); Writing – original draft (lead). **Wei Cui:** Funding acquisition (equal); Project administration (equal); Writing – review & editing (equal). **Tingting Gao:** Methodology (equal); Writing – review & editing (equal). **Shengyuan Liu:** Conceptualization (supporting). **Lin Zhao:** Funding acquisition (supporting); Resources (lead); Writing – review & editing (supporting). **Yaojun Ge:** Funding acquisition (equal); Resources (equal).

DATA AVAILABILITY

The data that support the findings of this study are available from the corresponding author upon reasonable request.

REFERENCES

Amman, O. H., Von Kármán, T., and Woodruff, G. B., "The failure of the Tacoma narrows bridge," Technical Report No. 105559175, 1941.

Balajewicz, M. and Dowell, E., "Reduced-order modeling of flutter and limit-cycle oscillations using the sparse volterra series," J. Aircr. **49**, 1803–1812 (2012).

Birnbaum, W., "Der schlagflügelpropeller und die kleinen schwingungen elastisch befestigter tragflügel," Z. Flugtech. Motorluftschiffahrt **15**, 128–134 (1924).

Brown, S. and Daniels, P., "On the viscous flow about the trailing edge of a rapidly oscillating plate," J. Fluid Mech. **67**, 743–761 (1975).

Brunton, S. L., Proctor, J. L., and Kutz, J. N., "Discovering governing equations from data by sparse identification of nonlinear dynamical systems," Proc. Natl. Acad. Sci. U. S. A. **113**, 3932–3937 (2016).

Chen, A., He, X., and Xiang, H., "Identification of 18 flutter derivatives of bridge decks," J. Wind Eng. Ind. Aerodyn. **90**, 2007–2022 (2002).

Chen, X., Matsumoto, M., and Kareem, A., "Time domain flutter and buffeting response analysis of bridges," J. Eng. Mech. **126**, 7–16 (2000).

Chen, Y., Wu, D., Duan, L., and Kang, Q., "Machine learning method for the supplement, correction, and prediction of the nonlinear dynamics in pattern formation," Phys. Fluids **33**, 024110 (2021).

Chen, Z., Yang, W., Li, J., Yi, T., Wu, J., and Wang, D., "Bridge influence line identification based on adaptive b-spline basis dictionary and sparse regularization," Struct. Control Health Monit. **26**, e2355 (2019).

Chu, X., Cui, W., Zhao, L., and Ge, Y., "Life-cycle assessment of long-span bridge's wind resistant performance considering multisource time-variant effects and uncertainties," J. Struct. Eng. **148**, 04022092 (2022).

Curtiss, H. C., Jr., Scanlan, R. H., and Sisto, F., *A Modern Course in Aeroelasticity* (Springer Science & Business Media, 2013), Vol. 11.

Denegri, C. M., Jr., "Limit cycle oscillation flight test results of a fighter with external stores," J. Aircr. **37**, 761–769 (2000).

Diana, G., Bruni, S., and Rocchi, D., "A numerical and experimental investigation on aerodynamic non linearities in bridge response to turbulent wind," EACWE **4**, 86 (2005).

Diana, G., Resta, F., Zasso, A., Belloli, M., and Rocchi, D., "Forced motion and free motion aeroelastic tests on a new concept dynamometric section model of the messina suspension bridge," J. Wind Eng. Ind. Aerodyn. **92**, 441–462 (2004).

Diana, G., Rocchi, D., Argentini, T., and Muggiasca, S., "Aerodynamic instability of a bridge deck section model: Linear and nonlinear approach to force modeling," J. Wind Eng. Ind. Aerodyn. **98**, 363–374 (2010).

Dinyavari, M. and Friedmann, P., "Application of time-domain unsteady aerodynamics to rotary-wing aeroelasticity," AIAA J. **24**, 1424–1432 (1986).

Ellington, C. P., "The aerodynamics of hovering insect flight. IV. Aerodynamic mechanisms," Philos. Trans. R. Soc. London, Ser. B **305**, 79–113 (1984).

Falco, M., Curami, A., and Zasso, A., "Nonlinear effects in sectional model aeroelastic parameters identification," J. Wind Eng. Ind. Aerodyn. **42**, 1321–1332 (1992).

Fang, G., Cao, J., Yang, Y., Zhao, L., Cao, S., and Ge, Y., "Experimental uncertainty quantification of flutter derivatives for a pk section girder and its application on probabilistic flutter analysis," J. Bridge Eng. **25**, 04020034 (2020).

Gu, M., Zhang, R., and Xiang, H., "Identification of flutter derivatives of bridge decks," J. Wind Eng. Ind. Aerodyn. **84**, 151–162 (2000).

Gülçat, Ü., *Fundamentals of Modern Unsteady Aerodynamics* (Springer, 2010).

von Karman, T. H. and Sears, W. R., "Airfoil theory for non-uniform motion," J. Aeronaut. Sci. **5**, 379–390 (1938).

Klus, S., Nüske, F., Koltai, P., Wu, H., Kevrekidis, I., Schütte, C., and Noé, F., "Data-driven model reduction and transfer operator approximation," J. Nonlinear Sci. **28**, 985–1010 (2018).

Klus, S., Nüske, F., Peitz, S., Niemann, J.-H., Clementi, C., and Schütte, C., "Data-driven approximation of the Koopman generator: Model reduction, system identification, and control," Physica D **406**, 132416 (2020).

Kou, J. and Zhang, W., "Data-driven modeling for unsteady aerodynamics and aeroelasticity," Prog. Aerosp. Sci. **125**, 100725 (2021).

Li, G., "On the post-flutter state of cable-stayed bridges," in *Cable Stayed Bridges* (ASCE, 1988) pp. 1–11.

Li, K., Kou, J., and Zhang, W., "Deep neural network for unsteady aerodynamic and aeroelastic modeling across multiple Mach numbers," Nonlinear Dyn. **96**, 2157–2177 (2019).

Li, K., Kou, J., and Zhang, W., "Unsteady aerodynamic reduced-order modeling based on machine learning across multiple airfoils," Aerosp. Sci. Technol. **119**, 107173 (2021).

Li, S., Kaiser, E., Laima, S., Li, H., Brunton, S. L., and Kutz, J. N., "Discovering time-varying aerodynamics of a prototype bridge by sparse identification of nonlinear dynamical systems," Phys. Rev. E **100**, 022220 (2019).

Li, T., Wu, T., and Liu, Z., "Nonlinear unsteady bridge aerodynamics: Reduced-order modeling based on deep LSTM networks," J. Wind Eng. Ind. Aerodyn. **198**, 104116 (2020).

Li, W., Laima, S., Jin, X., Yuan, W., and Li, H., "A novel long short-term memory neural-network-based self-excited force model of limit cycle oscillations of nonlinear flutter for various aerodynamic configurations," Nonlinear Dyn. **100**, 2071–2087 (2020).

Liu, S., Zhao, L., Fang, G., Hu, C., and Ge, Y., "Investigation on aerodynamic force nonlinear evolution for a central-slotted box girder under torsional vortex-induced vibration," J. Fluids Struct. **106**, 103380 (2021).

Liu, S., Zhao, L., Fang, G., Hu, C., and Ge, Y., "Nonlinear aerodynamic characteristics and modeling of a quasi-flat plate at torsional vibration: Effects of angle of attack and vibration amplitude," Nonlinear Dyn. **107**, 2027 (2022).

Marzocca, P., Silva, W. A., and Librescu, L., "Nonlinear open-/closed-loop aeroelastic analysis of airfoils via Volterra series," AIAA J. **42**, 673–686 (2004).

Muravleva, E., Oseledets, I., and Koroteev, D., "Application of machine learning to viscoplastic flow modeling," Phys. Fluids **30**, 103102 (2018).

Noda, M., Utsunomiya, H., Nagao, F., Kanda, M., and Shiraishi, N., "Effects of oscillation amplitude on aerodynamic derivatives," J. Wind Eng. Ind. Aerodyn. **91**, 101–111 (2003).

Pawar, S., Ahmed, S. E., San, O., and Rasheed, A., "Data-driven recovery of hidden physics in reduced order modeling of fluid flows," Phys. Fluids **32**, 036602 (2020).

Pawar, S., San, O., Aksoylu, B., Rasheed, A., and Kvamsdal, T., "Physics guided machine learning using simplified theories," Phys. Fluids **33**, 011701 (2021).

Prandtl, L., "Über die entstehung von wirbeln in der idealen flüssigkeit, mit anwendung auf die tragflügeltheorie und andere aufgaben," in *Vorträge aus Dem Gebiete Der Hydro-Und Aerodynamik (Innsbruck 1922)* (Springer, 1924), pp. 18–33.

Qiao, B., Zhang, X., Wang, C., Zhang, H., and Chen, X., "Sparse regularization for force identification using dictionaries," J. Sound Vib. **368**, 71–86 (2016).

Sarkar, P. P., Jones, N. P., and Scanlan, R. H., "System identification for estimation of flutter derivatives," J. Wind Eng. Ind. Aerodyn. **42**, 1243–1254 (1992).

Scanlan, R. H., "Observations on low-speed aeroelasticity," J. Eng. Mech. **128**, 1254–1258 (2002).

Scanlan, R. H. and Tomko, J. J., "Airfoil and bridge deck flutter derivatives," J. Eng. Mech. Div. **97**, 1717–1737 (1971).

de Silva, B. M., Higdon, D. M., Brunton, S. L., and Kutz, J. N., "Discovery of physics from data: Universal laws and discrepancies," Front. Artif. Intell. **3**, 25 (2020).

Su, W., Bogdan, M., and Candes, E., "False discoveries occur early on the lasso path," Ann. Stat. **45**, 2133–2150 (2017).

Taha, H. and Rezaei, A. S., "Viscous extension of potential-flow unsteady aerodynamics: The lift frequency response problem," J. Fluid Mech. **868**, 141–175 (2019).

Theodorsen, T. and Mutchler, W., "General theory of aerodynamic instability and the mechanism of flutter," Technical Report No. 496, 1935.

Thomas, J. P., Dowell, E. H., and Hall, K. C., "Nonlinear inviscid aerodynamic effects on transonic divergence, flutter, and limit-cycle oscillations," AIAA J. **40**, 638–646 (2002).

Tibshirani, R., "Regression shrinkage and selection via the lasso," J. R. Stat. Soc.: Ser. B **58**, 267–288 (1996).

de Visser, C., Mulder, J., and Chu, Q., "Global nonlinear aerodynamic model identification with multivariate splines," AIAA Paper No. 2009-5726, 2009.

Wagner, H., "Über die entstehung des dynamischen auftriebes von tragflügeln," Z. Angew. Math. Mech. **5**, 17 (1925).

Wang, C. and Eldredge, J. D., "Low-order phenomenological modeling of leading-edge vortex formation," Theor. Comput. Fluid Dyn. **27**, 577–598 (2013).

Wu, P., Sun, J., Chang, X., Zhang, W., Arcucci, R., Guo, Y., and Pain, C. C., "Data-driven reduced order model with temporal convolutional neural network," Comput. Methods Appl. Mech. Eng. **360**, 112766 (2020).

Wu, T. and Kareem, A., "Vortex-induced vibration of bridge decks: Volterra series-based model," J. Eng. Mech. **139**, 1831–1843 (2013).

Xia, X. and Mohseni, K., "Unsteady aerodynamics and vortex-sheet formation of a two-dimensional airfoil," J. Fluid Mech. **830**, 439–478 (2017).

Yang, Z. and Zhao, L., "Analysis of limit cycle flutter of an airfoil in incompressible flow," J. Sound Vibration **123**, 1–13 (1988).

Yao, W. and Marques, S., "Nonlinear aerodynamic and aeroelastic model reduction using a discrete empirical interpolation method," AIAA J. **55**, 624–637 (2017).

Yuan, M. and Lin, Y., "Model selection and estimation in regression with grouped variables," J. R. Stat. Soc.: Ser. B **68**, 49–67 (2006).

Zhang, M., Xu, F., and Han, Y., "Assessment of wind-induced nonlinear post-critical performance of bridge decks," J. Wind Eng. Ind. Aerodyn. **203**, 104251 (2020).

Zhao, L., Xie, X., Zhan, Y.-Y., Cui, W., Ge, Y.-J., Xia, Z.-C., Xu, S.-Q., and Zeng, M., "A novel forced motion apparatus with potential applications in structural engineering," J. Zhejiang Univ.-Sci. A **21**, 593–608 (2020).